



HAL
open science

A micromechanical muUNSAT effective stress expression for stress-strain behaviour of wet granular materials

Jérôme Duriez, R. Wan

► To cite this version:

Jérôme Duriez, R. Wan. A micromechanical muUNSAT effective stress expression for stress-strain behaviour of wet granular materials. *Geomechanics for Energy and the Environment*, 2018, 15, pp.10-18. 10.1016/j.gete.2017.12.003 . hal-01893074

HAL Id: hal-01893074

<https://hal.science/hal-01893074>

Submitted on 11 Oct 2018

HAL is a multi-disciplinary open access archive for the deposit and dissemination of scientific research documents, whether they are published or not. The documents may come from teaching and research institutions in France or abroad, or from public or private research centers.

L'archive ouverte pluridisciplinaire **HAL**, est destinée au dépôt et à la diffusion de documents scientifiques de niveau recherche, publiés ou non, émanant des établissements d'enseignement et de recherche français ou étrangers, des laboratoires publics ou privés.

A micromechanical μ UNSAT effective stress expression for stress-strain behaviour of wet granular materials

J. Duriez^{a,b,*}, R. Wan^a

^aUniversity of Calgary, Calgary, AB, T2N 1N4, Canada

^bIrstea, UR RECOVER, F-13182 Aix-en-Provence, France

Abstract

The definition of an effective stress variable for idealized triphasic granular media as the contact stress arising from interparticle forces is examined through discrete element modelling computations in concert with appropriately derived analytical stress expressions based on homogenization. The latter take a more practical importance, in that they also circumvent the need for direct measurements of interparticle contact forces. Considering dry or pendular-regime conditions for slightly polydisperse dense and loose packings, the contact stress-strain behaviours in dry or wet conditions are compared along a variety of loading paths, depending on the level of plastic dissipation involved. The contact stress indeed emerges as an effective stress variable with a remarkable stress-strain character along contractant loading paths and for dense solid packings where the behaviour is close to be non-dissipative. Along more dilatant loading paths or for looser packings, plastic dissipation increases and the coincidence of the constitutive behaviour in both dry and triphasic conditions is restricted to the initial stages of the loading paths, limiting the applicability of the contact stress to the estimation of initial stiffnesses. The stark constitutive differences between the proposed effective stress and Bishop's stress are also highlighted.

Keywords: effective stress, Discrete Element Method (DEM), granular, pendular, μ UNSAT

*Corresponding author

Email address: jerome.duriez@irstea.fr (J. Duriez)

1. Introduction

Energy and Environmental Engineering operations require a precise mechanical description of multiphase porous media such as in oil and gas reservoirs, or partially water-saturated (unsaturated) soils. Obviously, the presence of various fluids within the pore space network of these multiphase materials greatly modifies their mechanical behaviour with respect to the dry (air-saturated) state which is well understood. For biphasic (or two-phase) porous media penetrated by a single pore fluid, a unified mechanical description by way of dry state constitutive models actually exists whatever the pore fluid and its pressure are following Terzaghi's and Biot's effective stress equations [1, 2]. Turning to triphasic (or three-phase) conditions with an immiscible fluid mixture, it would also be highly beneficial to extend this effective stress concept so that triphasic materials can be described by just inserting an adequate single effective stress into models designed for dry materials. In other words, the objective is to obtain a stress-strain-strength effective stress that would allow failure criterion and constitutive relations from dry conditions, all together, to be applied to triphasic conditions in order to easily predict limit stress states and strains. However, the exact determination of such a single effective stress has revealed to be highly challenging ever since the early Bishop's attempts [3].

When describing failure in triphasic media, it has been often possible to resort to an effective stress framework based on limit stress states according to dry shear strength criteria [4, 5, 6, 7, 8]. In these works, the effective stress is either phenomenologically deduced from Bishop's equation with appropriate expressions for χ coefficient [4, 7], or as the contact forces stress contribution which can be indirectly accessed by subtracting a so-called suction stress from the total stress [5, 6, 8]. The suction stress [5] encompasses all relevant stress contributions in triphasic materials, excluding the contact stress stemming from the contact forces between the solid grains of the skeleton, and can be identified for granular materials with the capillary stress since other physico-chemical forces are then negligible. As for the contact stress, the latter appears as a

31 logical stress-strength effective stress since pore water is reported to have little
32 or no influence onto the contact-scale local frictional threshold [9, 10], which
33 thus leads to unique limit states for the macroscopic contact stress and a unified
34 failure description irrespective of saturation.

35 Whereas in the biphasic case unique constitutive relations are related to
36 strains via Biot’s effective stress, no effective stress has yet been found that
37 would relate to strains in triphasic conditions through dry constitutive relations
38 [7]. As such, the application of an effective stress principle to triphasic materials
39 has often been challenged since Bishop himself [3], with alternate approaches
40 relying on total stress and another stress variable such as matric suction to de-
41 scribe unsaturated conditions using additional constitutive equations that are
42 specific to these triphasic conditions [11, 12]. A compromise may, nevertheless,
43 be found in that quasi-elastic behaviour, e.g. volume change along overconsoli-
44 dated oedometric loadings, may still be described in triphasic conditions using an
45 effective stress framework [4, 13, 14]. Recent micromechanical results by the au-
46 thors [8, 15] suggest that the same contact stress also enjoys such a quasi-elastic
47 strain-stress effective nature, in addition to its stress-strength character. This
48 seems to be indeed coherent because granular material strains derive from solid
49 particle relative displacements that relate to contact forces through a unique
50 contact law, irrespective of saturation.

51 The present work aims to provide new evidences that demonstrate the stress-
52 strain effective character of the contact stress in any regime showing small plastic
53 dissipation by considering a wide range of loading paths which were absent from
54 previous studies [8, 15].

55 It is further noted that direct measurements of contact forces and contact
56 stresses are still beyond reach in triphasic materials in spite of a current research
57 in the field [16]. To address this shortcoming, the present paper first recalls in
58 Section 2 the μ UNSAT expressions that enable one to indirectly access the con-
59 tact stress through capillary stresses and the fluid phase microstructures, whose
60 measurements appear to be more feasible thanks to e.g. computed tomography
61 [17, 18]. For the purpose of the paper, the choice is actually made to con-

62 sider a Discrete Element Method (DEM) model for wet granular materials [19],
 63 presented in Section 3, which allows both direct and indirect measurements of
 64 the contact stress from a comprehensive description of the microstructure of all
 65 solid and fluid phases, including interfaces. Numerical comparisons of dry-wet
 66 behaviours for slightly polydisperse materials along various loading paths are
 67 then presented in Section 4, validating the stress-strain effective nature of the
 68 contact stress in regimes with small dissipation, and hence the present μ UNSAT
 69 effective stress expression. Section 5 finally evidences the fundamental differ-
 70 ences in the pendular regime between the present μ UNSAT effective stress and
 71 Bishop’s stress, whose inapplicability to wet conditions is once again demon-
 72 strated.

73 2. Micromechanical μ UNSAT effective stress expression

74 2.1. Total stress decomposition from micromechanics

75 The μ UNSAT approach expresses the contact stress by isolating from the
 76 macroscopic total stresses Σ , all microscopic stress contributions due to the
 77 various phases and interfaces that encompass triphasic granular media. First,
 78 the solid s and fluid (n, w) bulk phases are considered with their corresponding
 79 volumes V_s, V_n and V_w . Here, n stands for the non-wetting fluid, e.g. air,
 80 whereas w refers to the wetting one, e.g. water. Additionally, all three interfaces
 81 $S_{\alpha\beta}$, $\alpha, \beta = n, s, w$ are as well included in the approach since the corresponding
 82 surface tensions $\gamma_{\alpha\beta}$ necessarily belong to the internal forces of the triphasic
 83 material. As such, the total stresses are given as follows:

$$84 \quad \Sigma = \frac{1}{V} \left(\sum_{\alpha=n,s,w} \int_{V_\alpha} \sigma_\alpha dV + \sum_{\alpha,\beta=n,s,w} \int_{S_{\alpha\beta}} \pi_{\alpha\beta} dS \right) \quad (1)$$

85 In Eq. (1), the fluid stresses σ_α , $\alpha = n, w$, are directly given by the corre-
 86 sponding pressures $u_\alpha \delta$ with δ as the identity tensor, whereas the solid stress
 87 σ_s can be classically expressed in terms of the tractions acting along the solid
 88 particles surfaces S_p [20]. The surface stress tensors $\pi_{\alpha\beta} = \gamma_{\alpha\beta} (\vec{n} \otimes \vec{n} - \delta)$,
 89 with \vec{n} as the normal to $S_{\alpha\beta}$, finally describe the surface tension fields acting as
 internal forces within any interface $S_{\alpha\beta}$ [21, 22, 23, 24].

90 Algebraic manipulations applied to Eq. (1) lead to the following μ UNSAT
 91 decomposition of Σ into the contact stress σ^{cont} and the capillary stress σ^{cap} ,
 92 to which the solid fluid surface tensions $\gamma_{s\alpha}$ eventually do not contribute in the
 93 case of rigid solid particles [20, 22, 24]:

$$\Sigma - u_n \delta = \sigma^{cont} + \sigma^{cap} \quad (2)$$

$$\sigma^{cont} = \frac{1}{V} \sum_c \vec{f}^c \otimes \vec{l} \quad (3)$$

$$\begin{aligned} \sigma^{cap} &= -\frac{1}{V} \left[u_c \left(V_w \delta + \int_{S_{sw}} \vec{n} \otimes \vec{x} dS \right) \right. \\ &\quad \left. + \gamma_{nw} \left(\int_{S_{nw}} (\delta - \vec{n} \otimes \vec{n}) dS + \int_{\Gamma} \vec{\nu} \otimes \vec{x} dl \right) \right] \\ &= -\frac{1}{V} \left[u_c (\boldsymbol{\mu}_{Vw} + \boldsymbol{\mu}_{Ssw}) + \gamma_{nw} (\boldsymbol{\mu}_{Snw} + \boldsymbol{\mu}_{\Gamma}) \right] \quad (4) \end{aligned}$$

94 Eq. (3) refers to the standard definition of the contact stress tensor σ^{cont}
 95 from the contact forces \vec{f}^c between solid particles, and the corresponding branch
 96 vector \vec{l} connecting the centroids of contacting particles.

97 In Eq. (4), the capillary stress σ^{cap} encompasses the remainder of the in-
 98 ternal forces that arise both from the fluid-fluid surface tension γ_{nw} and the
 99 capillary pressure $u_c = u_n - u_w$ that is equal to suction in granular materials.
 100 Four microstructure tensors $\boldsymbol{\mu}_X$ reflect the tensorial nature of these internal
 101 forces, with $\boldsymbol{\mu}_{Vw}$ the only one being always spherical since it corresponds to
 102 the isotropic action of suction within V_w . Other microstructure tensors have
 103 a general, non-spherical, tensorial expression with e.g. $\boldsymbol{\mu}_{Ssw}$ depending on the
 104 orientation of the wetted surface S_{sw} since the latter sustains suction along its
 105 normal only. Also, $\boldsymbol{\mu}_{Snw}$, $\boldsymbol{\mu}_{\Gamma}$ reflect the orientations of the interface S_{nw} and of
 106 the three-phase contact lines Γ that are subjected to fluid-fluid surface tension,
 107 where $\vec{\nu}$ in Eq. (4) is the tangent to S_{nw} being normal to Γ [20].

108 2.2. μ UNSAT contact stress expression

109 Isolating σ^{cont} in Eq. (2)-(4), the following μ UNSAT expression for the
 110 contact stress is eventually obtained:

$$\sigma^{cont} = \Sigma - u_n \delta + \frac{1}{V} \left[u_c (\boldsymbol{\mu}_{Vw} + \boldsymbol{\mu}_{Ssw}) + \gamma_{nw} (\boldsymbol{\mu}_{Snw} + \boldsymbol{\mu}_{\Gamma}) \right] \quad (5)$$

111 Such an expression is believed to provide an easier access to σ^{cont} during ex-
 112 periments than the direct definition of Eq. (3). Imaging techniques such as
 113 computed tomography indeed are very promising in allowing precise measure-
 114 ments of the fluid phase microstructures [17, 18]. Then, one would be able
 115 to compute the microstructure tensors $\mu_{\mathbf{x}}$ in Eq. (5), as opposed to requiring
 116 more complex contact force measurements [16] that enter the direct contact
 117 stress expression, Eq. (3).

118 Leaving any experimental endeavour aside for now, Eq. (5) is herein used
 119 within the framework of DEM to investigate the very role of the contact stress
 120 in connection with strains, and whether it may serve as a strain-stress-strength
 121 effective stress expression.

122 3. DEM multiscale modelling of triphasic granular materials

123 Numerical DEM models indeed provide a convenient multiscale description
 124 of triphasic granular materials whereby the microstructure of all solid and fluid
 125 phases is easily measured. As such, the contact stress can be readily estimated
 126 using either Eq. (3) or (5) along various loading paths and for different packings.

127 3.1. Model formulation

128 Previously proposed in [19] and implemented in the Yade code [25], the
 129 considered DEM model addresses the case of spherical solid particles and a
 130 wetting fluid distribution in terms of distinct capillary bridges, i.e. menisci be-
 131 tween particles pairs (Fig. 1), in accordance with the so-called pendular regime,
 132 also referred to as wet conditions. Such conditions correspond to a low wetting
 133 saturation, S_w , only, where S_w is defined as:

$$S_w = \frac{V_w}{V_w + V_n} \quad (6)$$

134

135 In line with another DEM approach [26], the model does not compute any
 136 biphasic pore flow, but instead assumes thermodynamic equilibrium and uni-
 137 form capillary pressure conditions. As such, the menisci properties are computed

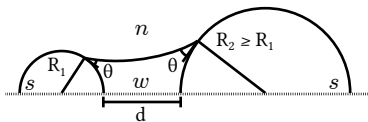


Figure 1: A capillary bridge

138 from the following Laplace-Young equation (7) which relates capillary pressure
 139 to surface tension and the interface curvature $\text{div}(\vec{n})$, with \vec{n} being the normal
 140 to S_{nw} pointing from n to w :

$$u_c = \gamma_{nw} \text{div}(\vec{n}) \quad (7)$$

141 According to the thermodynamic equilibrium assumption, Eq. (7) is solved
 142 for uniform values of u_c throughout the sample, also considering a uniform and
 143 constant contact angle θ (Fig. 1) [19]. As discussed in greater depth in [19],
 144 Eq. (7) is actually solved depending on the particles radii and their distance, in
 145 addition to imposed u_c and θ . Based on the S_{nw} interface profile, the numerical
 146 solution procedure finally outputs the resultant capillary force \vec{f}^{cap} and other
 147 relevant microstructural quantities such as $\mu_{S_{nw}} = \int_{S_{nw}} (\delta - \vec{n} \otimes \vec{n}) dS$ for
 148 instance, thus enabling one to apply the μ UNSAT Eq. (5) and measure contact
 149 stresses during DEM simulations [19].

150 The model actually inserts capillary bridges at each new contact between
 151 solid particles, with properties given by the Laplace-Young equation. In the
 152 instance the particles subsequently separate, the capillary bridge remains until
 153 some limit distance beyond which the Laplace-Young equation does not yield
 154 any solution. This hysteretic mechanism of bridge formation and rupture is
 155 consistent with experimental observations [27] and occurs in the model in a
 156 fully drained manner. The presence of a capillary bridge between two particles
 157 corresponds to a capillary interaction with the corresponding attractive capillary
 158 force \vec{f}^{cap} due to the capillary pressure and surface tension loadings along the
 159 wetted surfaces S_{sw} and the contact lines Γ .

160 In addition, the interaction between touching particles is governed by clas-
 161 sical elastic-plastic frictional (cohesionless) contact laws whereby normal and

162 tangential relative displacements between particles are restricted by normal and
 163 tangential contact forces f_n^c and f_t^c [8, 19]. A simplified linear elastic behaviour
 164 of the contact interaction is first defined by the normal and tangential local
 165 stiffnesses, k_n and k_t , which are directly obtained from the average diameter \bar{D}
 166 of any pair of contacting particles and the model parameters k_n/\bar{D} and k_t/k_n :

$$k_n = \frac{k_n}{\bar{D}} \bar{D} \quad (8)$$

$$k_t = \frac{k_t}{k_n} k_n \quad (9)$$

167 with the consideration of an elastic shear stiffness being eventually restricted by
 168 the following Coulombian friction threshold, with μ the friction coefficient:

$$|f_t^c| \leq \mu f_n^c \quad (10)$$

169 Table 1 lists all parameters of the DEM model. The retained values for the
 170 contact interaction parameters, k_n/\bar{D} and k_t/k_n , are similar to previous studies
 171 [8, 24, 19, 20]. As for the capillary interaction, the latter is fully determined
 172 by the fluid-fluid surface tension γ_{nw} , the contact angle θ and the particle size
 173 distribution. Air-water surface tension at ambient temperature is considered for
 174 γ_{nw} while a low though not zero θ -value corresponds to the wetting of glass beads
 175 by water, having at the same time the convenience of enhancing the mechanical
 176 effects of triphasic conditions [19]. Finally, silt-like particle diameters are chosen
 177 with a narrow particle size distribution being uniform in number between D_{min}
 178 and D_{max} .

Contact			Capillarity		Packing	
k_n/\bar{D}	k_t/k_n	μ	γ_{nw}	θ	D_{min}	D_{max}
(MPa)	(-)	(-)	(N/m)	(°)	(μm)	(μm)
10	0.5	0.5	0.073	10	21	25

Table 1: DEM model parameters

179 While the dynamic scheme of the DEM is classically carried out using some
 180 numerical damping, in order to obtain more easily a quasi-static evolution of the
 181 system, the damping coefficient [25] is taken as low as 0.05 to avoid numerical

182 artifacts. Quasi-staticity is systematically verified through low values of the
 183 particle unbalanced forces [25] which were below 1% during all loading cases.
 184 As such, particle inertia (mass) does not play any role in the computations,
 185 which allows the use of density scaling with an artificially high density value
 186 ($\rho = 20,000 \text{ kg/m}^3$ instead of $2,600 \text{ kg/m}^3$) for the particles. Without any
 187 consequence on the quasi-static rheology, density scaling reduces computational
 188 costs through larger time steps, even though loading rates have to be marginally
 189 reduced for quasi-staticity to still hold.

190 The DEM sample is a parallelepiped, initially a cube approximately 0.6 mm a
 191 side depending on packing density, with 6 rigid walls that enclose a total number
 192 of 20,000 spherical Discrete Elements (DE). Similar numbers (10,000 to 20,000)
 193 are classically used in material-scale DEM analyses [26, 19, 20, 28] in order to
 194 avoid numerical result dispersion from one numerical sample to another as well
 195 as field heterogeneity, in conformity with the Representative Elementary Volume
 196 (REV) concept. The DE sample is packed at various levels to produce different
 197 states in density as quantified by the porosity n and the average coordination
 198 number z_c :

$$n = \frac{V_n + V_w}{V_s + V_n + V_w} = \frac{V_v}{V} \quad (11)$$

$$z_c = \frac{2 N_c - N_1}{N_p - N_1 - N_0} \quad (12)$$

199 with N_c the total number of contacts, and $N_0 + N_1$ the number of excluded
 200 rattlers, i.e. particles with zero or only one contact, and N_p the total number of
 201 DE. All considered packings are initially isotropic and prepared such that dry
 202 vs wet comparisons can be conducted in an unbiased manner.

203 Care is indeed taken in considering dry or wet solid packings to be compara-
 204 ble in terms of n and z_c as these parameters obviously affect the dry constitutive
 205 relation which should also be described in wet conditions by an effective stress.
 206 As such, an appropriate particle packing generation procedure is followed which
 207 first involves a classical isotropic compression until a desired confining pressure
 208 is reached to obtain dense or loose dry packings [26], without the consideration
 209 of any capillary interaction that is only introduced in a second stage for the

210 wet samples. In this manner, wet packings show initial states which are barely
 211 affected by the presence of capillary forces, and thus compare well with dry
 212 packings.

213 3.2. Dry and wet strain proportional loading paths

214 In order to investigate the stress-strain effective nature of the contact stress,
 215 the DEM model is used to explore the existence of a unique constitutive relation
 216 \mathcal{F} between $\boldsymbol{\sigma}^{cont}$ and the strains $\boldsymbol{\varepsilon}$ in both dry (biphasic) and wet (triphasic)
 217 conditions. In the case of such an existence, \mathcal{F} by definition would relate the
 218 current contact stress $\boldsymbol{\sigma}^{cont}(t)$ to the strain loading path $[\boldsymbol{\varepsilon}(\tau); -\infty < \tau \leq t]$
 219 such that:

$$\boldsymbol{\sigma}^{cont}(t) = \mathcal{F}([\boldsymbol{\varepsilon}(\tau); -\infty < \tau \leq t]) \quad (13)$$

220 Extending our previous work [8, 15] where classical triaxial paths were exam-
 221 ined, the validity of the same Eq. (13) in dry and wet conditions with a unique
 222 \mathcal{F} is herein probed considering axisymmetric strain proportional loading paths,
 223 with ‘1’ as the axis of symmetry and ‘2,3’ the two other spatial directions:

$$d\varepsilon_1 = cst \geq 0 ; d\varepsilon_2 = d\varepsilon_3 ; d\varepsilon_1 + 2Rd\varepsilon_3 = 0 \quad (14)$$

224 The loading parameter $R \geq 0$ is constant along a given path, $R = 1$ corresponds
 225 to an isochoric loading path, whereas dilatancy (resp. contractancy) is imposed
 226 for $0 < R < 1$ (resp. $R > 1$). The limiting case $R = 0$ is defined as another
 227 contractant path ($d\varepsilon_1 = 0 ; d\varepsilon_2 = d\varepsilon_3 = cst \geq 0$).

228 Let’s denote the volumetric strain as ε_V :

$$\varepsilon_V = \varepsilon_1 + 2\varepsilon_3 \quad (15)$$

229 and choose $\|\boldsymbol{\varepsilon}\|$ (the Euclidean norm of $\boldsymbol{\varepsilon}$) as a monotonously increasing loading
 230 parameter, i.e.

$$\|\boldsymbol{\varepsilon}\| = \sqrt{\varepsilon_1^2 + 2\varepsilon_3^2} \quad (16)$$

231 Accordingly, Fig. 2 illustrates the corresponding dilatancy rates of four loading
 232 paths with $R \in \{0; 0.2; 1; 5\}$ that will be considered in the following analysis. In
 233 all cases, imposed strain rates are low enough to ensure quasi-static simulations

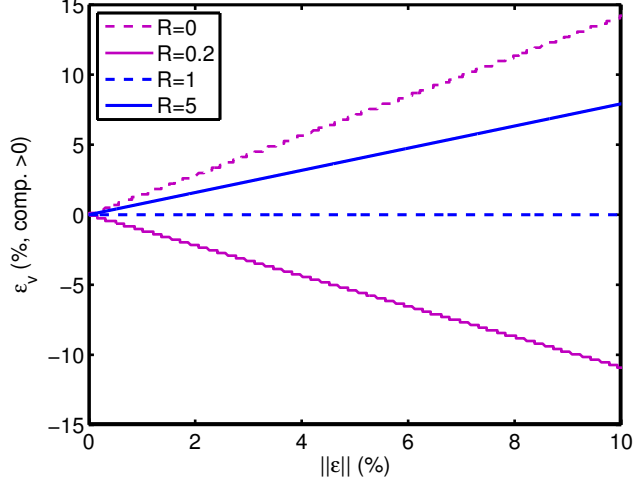


Figure 2: Dilatancy rates of imposed loading paths for $R \in \{0; 0.2; 1; 5\}$

234 as verified from the corresponding low values of the particle unbalanced forces
 235 [25] which were below 1%.

236 The main objective of imposing such strain loading paths on both dry and
 237 wet packings is to verify the hypothesis, $\boldsymbol{\sigma}' = \boldsymbol{\sigma}^{cont}$, upon which is founded
 238 the μ UNSAT framework. If Eq. (13) holds, then the resulting contact stress
 239 paths should coincide in both dry and wet conditions. Recognizing the axial
 240 symmetry of the problem, it is convenient to associate the tensor $\boldsymbol{\sigma}^{cont}$ with
 241 the two classical scalars (invariants) p^{cont} and q^{cont} , i.e.

$$p^{cont} = \frac{\sigma_1^{cont} + 2\sigma_3^{cont}}{3} \quad (17)$$

$$q^{cont} = \sigma_1^{cont} - \sigma_3^{cont} \quad (18)$$

242 while similarly, p and q variables pertain to the total stress tensor $\boldsymbol{\Sigma}$:

$$p = \frac{\Sigma_1 + 2\Sigma_3}{3} \quad (19)$$

$$q = \Sigma_1 - \Sigma_3 \quad (20)$$

243 **4. Validity of the μ UNSAT effective stress**

244 *4.1. Dense packings*

245 Proportional strain loading paths are first imposed to dense solid packings.
 246 In essence, the same strain loading path is imposed to similarly dense packings
 247 in both dry and wet conditions with the resulting contact stress paths recorded.
 248 The contact stress obviously coincides with the total stress in dry conditions,
 249 whereas Eq. (3) or (5) can be indistinctly used to access the contact stress under
 250 wet conditions [28].

251 Four strain loading paths are considered with $R \in \{0; 0.2; 1; 5\}$, under two
 252 different confining pressures referred to as “A” and “B”. For each confining
 253 pressure A or B, and each R value, one dry and one wet test are considered,
 254 leading to 16 tests on dense packings in total. Table 2 gives details of the initial
 255 conditions for the dry-wet test pairs A, B pertaining to dense packings. These
 256 initial conditions are such that dry and wet tests of a given pair A or B show
 257 initial states (σ^{cont}, n, z_c) being as close as possible.

	Tests A		Tests B	
	Dry	Wet	Dry	Wet
Initial p (kPa)	11.1	2	20.6	10
Imposed u_c (kPa)	—	25	—	125
Initial S_w (%)	—	7.18	—	0.85
Initial n (-)	0.375	0.380	0.370	0.373
Initial z_c (-)	6.41	6.21	6.62	6.52

Table 2: Tests data for the dry and wet loading paths imposed on dense packings

258 Comparing the contact stress responses in dry and wet conditions (Fig. 3
 259 and 4), it is indeed verified that virtually unique behaviours are observed along
 260 the contractant or isochoric loading paths $R \in \{0; 1; 5\}$. As such, this establishes
 261 the validity of using the dry constitutive relation \mathcal{F} together with σ^{cont} as an
 262 effective stress along these loading paths.

263 As for the dilatant loading path $R = 0.2$, a unique behaviour is observed in
 264 the early stage of the test. Subsequently, the imposed dilatancy rate requires the
 265 stresses to eventually vanish in the dry case, whereas when wet the same packing

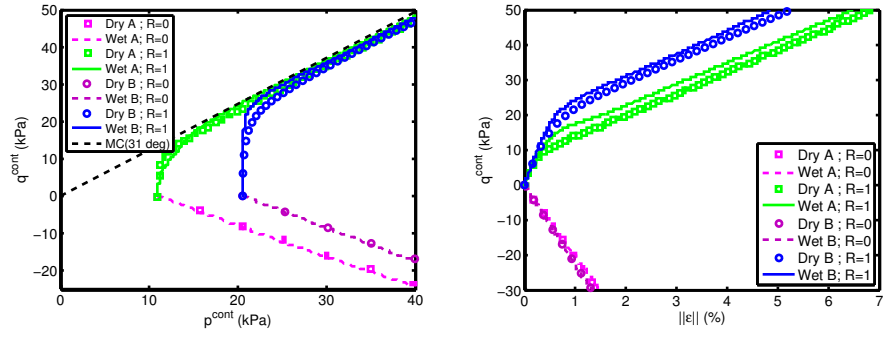


Figure 3: Contact stress response of a dense packing (Table 2) along contractant ($R = 0$) and isochoric ($R = 1$) strain loading paths (color version online)

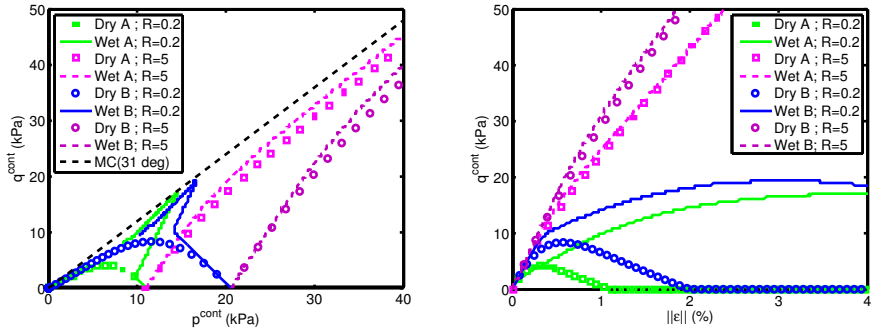


Figure 4: Contact stress response of a dense packing (Table 2) along contractant ($R = 5$) and dilatant ($R = 0.2$) strain loading paths (color version online)

266 gains a propensity to dilate originating from liquid bridges, thus avoiding a loss
 267 in bearing capacity. Hence, for such a dilatant loading path, the role of the
 268 contact stress as an effective stress is limited to the initial part of the loading
 269 path, and could still be used to predict initial stiffnesses in triphasic conditions.

270 It is noted that all contact stress responses obtained in both dry and triphasic
 271 conditions are found to be bounded by the same cohesionless Mohr-Coulomb
 272 failure criterion (with $c = 0$ Pa ; $\varphi = 31^\circ$) that was previously measured in
 273 dry conditions for such packings [15]. The universal property of this limit stress
 274 line, irrespective of the phase condition, is another illustration of the previously
 275 mentioned stress-strength effective nature of the contact stress.

276 4.2. Loose packing

277 The same analysis procedure is now applied to loose packings (Table 3). The
 278 numerical results displayed in Figs. 5 and 6 reveal less of an agreement between
 279 dry and wet behaviours in comparison to the previous dense case study.

	Tests A		Tests B	
	Dry	Wet	Dry	Wet
Initial p (kPa)	8.1	2	17.3	10
Imposed u_c (kPa)	—	25	—	125
Initial S_w (%)	—	4.17	—	0.50
Initial n (-)	0.442	0.441	0.436	0.438
Initial z_c (-)	4.96	4.84	5.17	5.12

Table 3: Tests data for the dry and wet loading paths imposed on loose packings

280 In particular, the existence of a unique constitutive relation \mathcal{F} between σ^{cont}
 281 and ε is identified for the most contractant loading path $R = 0$ only, and is
 282 somewhat approximated along the less contractant path $R = 5$.

283 As for the isochoric path $R = 1$, and at variance with the dense packing
 284 (Fig. 3), a dry-wet agreement is only obtained for the very initial phase during
 285 which p^{cont} remains constant, consistent with a possible relationship between
 286 σ^{cont} and ε through Hooke's elastic law. Then, the dry packing presents a
 287 'liquefaction' behaviour with vanishing stresses, consistent with the constant
 288 volume condition and the underlying material contractant flow rule. In contrast,

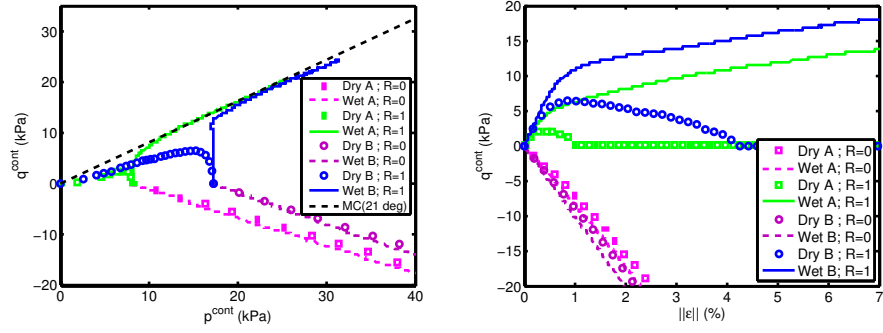


Figure 5: Contact stress response of a loose packing (Table 3) along contractant ($R = 0$) and isochoric ($R = 1$) strain loading paths (color version online)

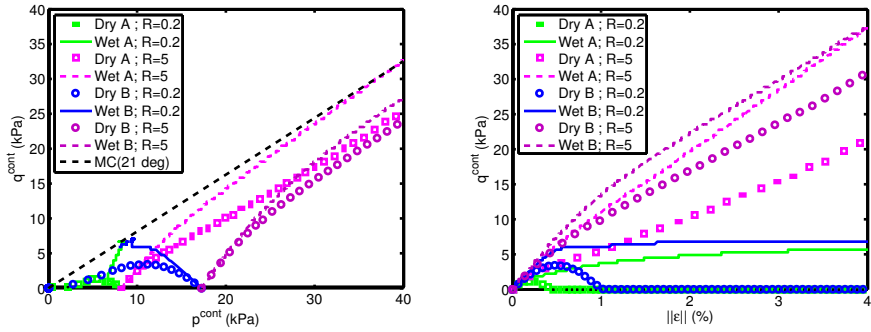


Figure 6: Contact stress response of a loose packing (Table 3) along contractant ($R = 5$) and dilatant ($R = 0.2$) strain loading paths (color version online)

289 similar packings under triphasic conditions gain a propensity to dilate due to
 290 liquid bridges, thus leading the mean contact stress to increase.

291 Some influence of the mean contact stress on the dry-wet comparison is
 292 finally observed along the dilatant loading path $R = 0.2$. Along such a path,
 293 dry conditions induce the stresses in this loose material to vanish as expected,
 294 while triphasic conditions enhance again the material dilatant nature, leading
 295 to non zero stress states. The exact behaviour of the wet material nevertheless
 296 depends on the confining pressure.

297 For a low confining pressure, the wet loose packing behaves similarly to the
 298 dense one because capillary stress plays an important part of the total stresses:
 299 $|p^{cap}|/p \approx 3.0$ and $|p^{cap}|/p^{cont} \approx 0.75$ at the initial stage of this test. The
 300 behaviour then changes into one with a greater propensity to dilate as a result
 301 of triphasic conditions.

302 On the other hand, upon increasing the confining pressure, the contact
 303 stress also increases while the capillary stress remains fairly constant, leading
 304 to $|p^{cap}|/p^{cont} \approx 0.42$ and $|p^{cap}|/p \approx 0.72$, initially. The changes in the rela-
 305 tive contributions from contact and capillary stresses diminish the liquid bridge
 306 induced dilatancy in the loose packing.

307 Finally, and as previously noted for the dense packing, the plastic limit
 308 criterion ($c = 0$ Pa ; $\varphi = 21^\circ$) corresponding to this loose material under dry
 309 conditions [15] also applies to the contact stress under triphasic conditions, once
 310 again confirming the stress-strength effective nature of σ^{cont} .

311 4.3. Discussion: effective stress vs dissipation and elasticity

312 The influences of the loading path and the solid packing on the ability of
 313 σ^{cont} to act as a stress-strain effective stress are now interpreted in relation to
 314 the variable dissipation associated with the observed behaviours. From f_n^c and
 315 f_t^c the normal and tangential components of the contact forces \vec{f}^c , the specific
 316 elastic energy e^{el} of the material is:

$$e^{el} = \frac{1}{2V} \sum_{N_c} \left(\frac{(f_n^c)^2}{k_n} + \frac{(f_t^c)^2}{k_t} \right) \quad (21)$$

317 which is easily measured from the DEM model, together with its increment
 318 δe^{el} between successive states. Comparing this increment with the incremental
 319 external work $\Sigma : d\boldsymbol{\varepsilon}$, the following quantity λ quantifies the deviation of the
 320 mechanical behaviour of any dry test from a non-dissipative behaviour:

$$\lambda = \left| \frac{\Sigma : d\boldsymbol{\varepsilon} - \delta e^{el}}{\Sigma : d\boldsymbol{\varepsilon}} \right| \quad (22)$$

321 The quasi-static nature of the loading paths ensures that both the kinetic energy
 322 and the energy term associated to numerical damping are negligible, and thus
 323 do not contribute to the energy balance quantified by the quantity λ . As such,
 324 during a non-dissipative, e.g. elastic, dry loading path, λ is equal to 0 throughout
 325 since all external work is completely stored as elastic energy. On the other hand,
 326 increasing values of λ reveal an increasing dissipation. It is noted that λ may
 327 be greater than 1 in the instance of elastic energy loss ($\delta e^{el} < 0$).

328 However, it is to stress out that a non-dissipative behaviour with negligi-
 329 ble values of λ does not necessarily correspond to a stress-strain path being
 330 reversible, even though the opposite is true. These intricacies are specific to
 331 granular materials whose elastic energy is contained in a contact network whose
 332 properties (for instance, N_c in Eq. (21)) fundamentally depend on irreversible
 333 strains. Also, granular materials are prone to irreversible yet non-dissipative
 334 local mechanisms such as contact losses. These very specific features can be
 335 interpreted in terms of a locked elastic energy concept [29] and have also been
 336 widely commented, e.g. in [30, 31], motivating here the distinction between the
 337 “non-dissipative” and “elastic” terminologies.

338 From the evolutions of λ shown in Figs. 7, and comparing with previous
 339 Figs. 3, it clearly appears that it is along the less dissipative loading paths that
 340 the stress-strain effective nature of $\boldsymbol{\sigma}^{cont}$ is the most marked, e.g. $R = 0$. Such
 341 a result includes and extends the finding previously reported in [4, 13] that an
 342 effective stress approach is possible in the elastic regime.

343 Another illustration of the role of dissipation in the effective stress discus-
 344 sion is proposed in Fig. 8 which considers an extreme case of the DEM model,
 345 referred to as $\mu = \infty$. In this extreme case of the DEM model, an ideal contact

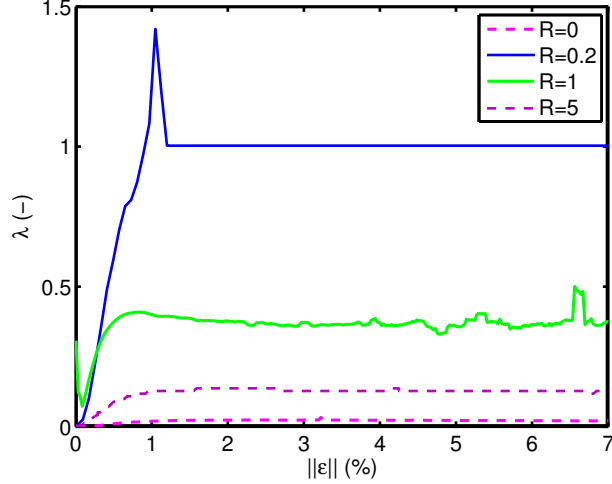


Figure 7: Dissipative nature of the behaviour during various dry loading paths imposed on the dense packing (Tests A). Raw data have been smoothed without altering the average trends and λ -values for $R=0.2$ may be disregarded beyond $\|\epsilon\| \approx 1\%$ since stresses vanish at this point

346 description is adopted in which no frictional threshold (10) limit is imposed on
 347 the shear contact force: f_t^c just evolves linearly with the tangential relative dis-
 348 placement according to the shear stiffness k_t as long as a contact exists. The
 349 dry-wet comparisons shown in Fig. 8 then reveal an enhanced stress-strain effec-
 350 tive character of σ^{cont} with this model, as opposed to the already discussed
 351 dry-wet comparisons with the classical friction coefficient $\mu = 0.5$ for the loose
 352 packing along the $R = 5$ loading path.

353 The present discussion finally sheds some light on the generality of ther-
 354 momechanical approaches to effective stress, as proposed e.g. in [23, 32, 33].
 355 Because the effective stress discussion herein appears to be widely different de-
 356 pending on the elastic or dissipative nature of the behaviour, and since such
 357 thermomechanical approaches usually rely on the assumption of an elastic be-
 358 haviour for the solid phase with an appropriate potential, it is probably impos-
 359 sible to generalize the conclusions obtained through thermomechanics outside
 360 the assumed framework.

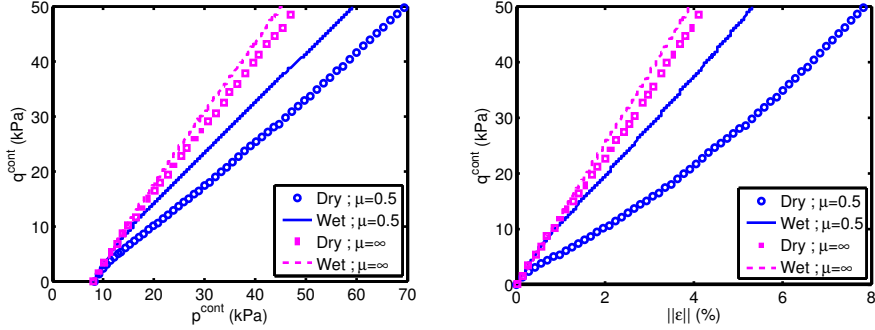


Figure 8: Influence of local friction μ on the contact stress' effective nature for a loose packing along a contractant loading path ($R = 5$)

5. Comparison with Bishop's stress

5.1. Qualitative discussion

The present μ UNSAT approach to effective stress is now compared with the commonly used effective stress expression as Bishop's stress σ^{Bish} :

$$\sigma' \stackrel{?}{=} \sigma^{Bish} = \Sigma - u_n \delta + u_c \chi \delta \quad (23)$$

Formally, significant differences appear between Bishop's equation (23) and the proposed μ UNSAT equation (5). It is herein recalled that the μ UNSAT equation includes a surface tension dependency in addition to that of capillary pressure, as well as the possibility of a non-spherical, microstructure-dependent, capillary stress contribution. Such features that characterize the microstructural details in triphasic materials go beyond the scope of Bishop's stress that relies on an average fluid pressure, being proportionnal to u_c and necessarily spherical. Since triphasic conditions by nature involve fluid-fluid interfaces and corresponding surface tension, the lack of γ^{nw} in Bishop's approach is questionable, as is the hypothesis of an averaged (isotropic) fluid pressure, while the wetted solid surfaces for instance experience capillary pressure along their normals only. Actually, the deviatoric nature of the capillary stresses has been repeatedly demonstrated in the pendular regime from modelling approaches [6, 26, 8, 24, 20], with possible variations in q^{cont} or q^{cap} independently of q

379 during microstructural changes of the fluid phases, contrary to Bishop’s general
 380 equality between q and q^{Bish} .

381 *5.2. Quantitative discussion*

382 In order to illustrate the inadequacy of Bishop’s stress to serve as an effective
 383 stress in the pendular regime, other dry-wet comparisons are presented for the
 384 dense packing along the two loading paths $R \in \{1; 5\}$, from initial states pre-
 385 sented in Table 4. The present discussion actually narrows down to the classical
 386 choice $\chi = S_w$ for Bishop’s parameter, which can be continuously measured
 387 during DEM simulations thanks to the complete description of the microstruc-
 388 ture. As such, the stress response observed in dry conditions is now compared
 389 to the Bishop’s stress response measured during triphasic conditions along the
 390 same strain paths.

	Dry	Wet
Initial p (kPa)	11.5	10
Imposed u_c (kPa)	—	125
Initial S_w (%)	—	0.85
Initial n (-)	0.375	0.373
Initial z_c (-)	6.41	6.52

Table 4: Tests data for the dry-wet comparison in terms of Bishop’s stress

391 Such loading paths $R \in \{1; 5\}$ revealed a very good agreement of the $\sigma^{cont-\epsilon}$
 392 behaviours in both dry and wet conditions (Figs. 3 and 4). However, the wet
 393 behaviour in terms of Bishop’s stress here significantly deviates from the dry be-
 394 haviour (Fig. 9), clearly showing that Bishop’s stress is a much less appropriate
 395 effective stress measure along these loading paths than the contact stress. In
 396 addition to this degraded stress-strain effective character of Bishop’s stress, it
 397 is also clear from the present comparison that Bishop’s stress is also inadequate
 398 to describe the strength of wet materials from the dry plastic limit criterion,
 399 which σ^{Bish} violates. The consideration of Bishop’s stress in an effective stress
 400 approach with some dry shear strength criterion in practice would thus lead
 401 to an overestimation of the risk of material failure in the pendular regime, in

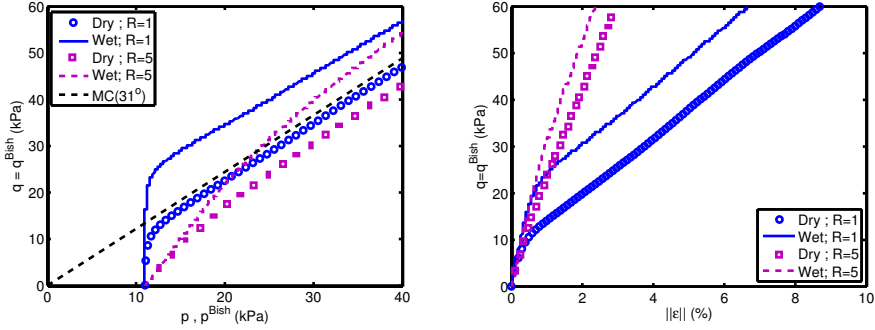


Figure 9: Bishop’s or total stress responses along isochoric ($R = 1$) and contractant ($R = 5$) loading paths imposed on a dense packing

402 connection with an underestimation of capillary stresses already discussed in
 403 [20, 24].

404 6. Conclusion

405 Micromechanical modelling approaches showed evidence of a single effective
 406 stress variable that can be used together with dry constitutive relations
 407 to describe the strains of idealized slightly polydisperse granular media in the
 408 pendular regime. The appropriate variable is the contact stress whose direct
 409 evaluation requires the prior knowledge of the contact force network. Using
 410 the proposed μ UNSAT expression, contact stresses can be alternatively calcu-
 411 lated through measurements or estimations of the fluid phase microstructure
 412 (interconnects), which are easier to determine than forces.

413 Unique contact stress-strain relationships have indeed been numerically demon-
 414 strated along a variety of loading paths for both dry and wet (pendular regime)
 415 conditions. This lends strong support to applying the effective stress designa-
 416 tion to contact stress. However, the considered loading paths have to induce
 417 small dissipation for the stress-strain effective stress approach to hold. Namely,
 418 contractant loading paths and dense packings are well suited for the application
 419 of the present μ UNSAT approach to hold.

420 Previous experimental and phenomenological works by [4, 13] had restricted
 421 the existence of a single stress-strain effective stress in triphasic media to the

422 elastic regime. This work based on microstructural analysis suggests a less
423 restrictive condition by extending it to even the irreversible regime but with
424 small dissipation.

425 There remain open questions as to whether new definitions of strain quan-
426 tities could cast the presented results into an even more general framework.
427 The present approach actually relies on observable strains or particle relative
428 displacements that are due to both contact and capillary forces, through the
429 classical DEM workflow (second Newton’s law). Alternatively, it could be at-
430 tempted to define distinct, non-observable, strain components: first, a contact
431 strain uniquely caused by contact forces, and second, a capillary strain uniquely
432 due to capillary forces, with the combination of the two leading to the ob-
433 servable strains herein considered. Such an alternative framework may lead to
434 strictly unique constitutive relations between the contact stress and such a con-
435 tact strain, and shed some light on the dissipation role through the yet to be
436 defined link between contact strain and observable strain.

437 **Acknowledgements**

438 This work has been funded by the Natural Science and Engineering Research
439 Council of Canada and Foundation Computer Modelling Group.

- 440 [1] K. Terzaghi, The shearing resistance of saturated soils and the angle be-
441 tween the planes of shear, in: Proceedings of the 1st International con-
442 ference on soil mechanics and foundation engineering, Vol. 1, Cambridge,
443 1936, pp. 54–56.
- 444 [2] M. A. Biot, General theory of three-dimensional consolidation, *Journal of*
445 *Applied Physics* 12 (2) (1941) 155–164. doi:10.1063/1.1712886.
- 446 [3] A. W. Bishop, G. E. Blight, Some aspects of effective stress in saturated
447 and partly saturated soils, *Géotechnique* 13 (1963) 177–197.
- 448 [4] N. Khalili, F. Geiser, G. Blight, Effective stress in unsaturated soils: Review

- 449 with new evidence, *International Journal of Geomechanics* 4 (2) (2004) 115–
450 126. [doi:10.1061/\(ASCE\)1532-3641\(2004\)4:2\(115\)](https://doi.org/10.1061/(ASCE)1532-3641(2004)4:2(115)).
- 451 [5] N. Lu, W. Likos, Suction stress characteristic curve for unsaturated soil,
452 *Journal of Geotechnical and Geoenvironmental Engineering* 132 (2) (2006)
453 131–142. [doi:10.1061/\(ASCE\)1090-0241\(2006\)132:2\(131\)](https://doi.org/10.1061/(ASCE)1090-0241(2006)132:2(131)).
- 454 [6] P.-Y. Hicher, C. Chang, A microstructural elastoplastic model for unsat-
455 urated granular materials, *International Journal of Solids and Structures*
456 44 (7-8) (2007) 2304 – 2323. [doi:10.1016/j.ijsolstr.2006.07.007](https://doi.org/10.1016/j.ijsolstr.2006.07.007).
- 457 [7] M. Nuth, L. Laloui, Effective stress concept in unsaturated soils: Clar-
458 ification and validation of a unified framework, *International Journal for*
459 *Numerical and Analytical Methods in Geomechanics* 32 (7) (2008) 771–801.
460 [doi:10.1002/nag.645](https://doi.org/10.1002/nag.645).
- 461 [8] R. Wan, J. Duriez, F. Darve, A tensorial description of stresses in tripha-
462 sic granular materials with interfaces, *Geomechanics for Energy and the*
463 *Environment* 4 (2015) 73–87. [doi:10.1016/j.gete.2015.11.004](https://doi.org/10.1016/j.gete.2015.11.004).
- 464 [9] I. Cavarretta, I. Rocchi, M. Coop, A new interparticle friction apparatus
465 for granular materials, *Canadian Geotechnical Journal* 48 (12) (2011) 1829–
466 1840. [doi:10.1139/t11-077](https://doi.org/10.1139/t11-077).
- 467 [10] K. Senetakis, M. R. Coop, M. C. Todisco, The inter-particle coefficient of
468 friction at the contacts of leighton buzzard sand quartz minerals, *Soils and*
469 *Foundations* 53 (5) (2013) 746–755. [doi:10.1016/j.sandf.2013.08.012](https://doi.org/10.1016/j.sandf.2013.08.012).
- 470 [11] D. G. Fredlund, N. R. Morgenstern, R. A. Widger, The shear strength of
471 unsaturated soils, *Canadian Geotechnical Journal* 15 (3) (1978) 313–321.
472 [doi:10.1139/t78-029](https://doi.org/10.1139/t78-029).
- 473 [12] E. E. Alonso, A. Gens, A. Josa, A constitutive model for partially saturated
474 soils, *Géotechnique* 40 (3) (1990) 405–430.

- 475 [13] E. Alonso, J.-M. Pereira, J. Vaunat, S. Olivella, A microstructurally based
476 effective stress for unsaturated soils, *Géotechnique* 60 (2010) 913–925(12).
477 [doi:10.1680/geot.8.P.002](https://doi.org/10.1680/geot.8.P.002).
- 478 [14] W. Baille, S. Tripathy, T. Schanz, Effective stress in clays of various min-
479 eralogy, *Vadose Zone Journal* 13 (5). [doi:10.2136/vzj2013.06.0112](https://doi.org/10.2136/vzj2013.06.0112).
- 480 [15] J. Duriez, R. Wan, M. Pouragha, Partially saturated granular ma-
481 terials: Insights from micro-mechanical modelling, in: *Proceedings*
482 *of the 6th Biot Conference on Poromechanics, 2017*, pp. 441–448.
483 [doi:10.1061/9780784480779.054](https://doi.org/10.1061/9780784480779.054).
- 484 [16] R. Hurley, E. Marteau, G. Ravichandran, J. E. Andrade, Extracting
485 inter-particle forces in opaque granular materials: Beyond photoelastic-
486 ity, *Journal of the Mechanics and Physics of Solids* 63 (2014) 154 – 166.
487 [doi:10.1016/j.jmps.2013.09.013](https://doi.org/10.1016/j.jmps.2013.09.013).
- 488 [17] K. A. Culligan, D. Wildenschild, B. S. B. Christensen, W. G. Gray,
489 M. L. Rivers, A. F. B. Tompson, Interfacial area measurements for unsat-
490 urated flow through a porous medium, *Water Resources Research* 40 (12).
491 [doi:10.1029/2004WR003278](https://doi.org/10.1029/2004WR003278).
- 492 [18] J.-F. Bruchon, J.-M. Pereira, M. Vandamme, N. Lenoir, P. Delage, X-ray
493 microtomography characterisation of the changes in statistical homogene-
494 ity of an unsaturated sand during imbibition, *Géotechnique Letters* 3 (2)
495 (2013) 84–88. [doi:10.1680/geolett.13.00013](https://doi.org/10.1680/geolett.13.00013).
- 496 [19] J. Duriez, R. Wan, Contact angle mechanical influence for
497 wet granular soils, *Acta Geotechnica* 12 (1) (2017) 67–83.
498 [doi:10.1007/s11440-016-0500-6](https://doi.org/10.1007/s11440-016-0500-6).
- 499 [20] J. Duriez, M. Eghbalian, R. Wan, F. Darve, The micromechanical
500 nature of stresses in triphasic granular media with interfaces,
501 *Journal of the Mechanics and Physics of Solids* 99 (2017) 495–511.
502 [doi:10.1016/j.jmps.2016.10.011](https://doi.org/10.1016/j.jmps.2016.10.011).

- 503 [21] M. E. Gurtin, A. I. Murdoch, A continuum theory of elastic material sur-
504 faces, *Archive for Rational Mechanics and Analysis* 57 (4) (1975) 291–323.
505 [doi:10.1007/BF00261375](https://doi.org/10.1007/BF00261375).
- 506 [22] X. Chateau, L. Dormieux, Homogenization of a non-saturated porous
507 medium: Hill’s lemma and applications, *C. R. Acad. Sci. Paris, Série II*
508 320 (1995) 627–634.
- 509 [23] W. G. Gray, B. A. Schrefler, Analysis of the solid phase stress tensor in mul-
510 tiphase porous media, *International Journal for Numerical and Analytical*
511 *Methods in Geomechanics* 31 (4) (2007) 541–581. [doi:10.1002/nag.541](https://doi.org/10.1002/nag.541).
- 512 [24] J. Duriez, R. Wan, Stress in wet granular media with interfaces via ho-
513 mogenization and discrete element approaches, *Journal of Engineering Me-*
514 *chanics* 142 (12). [doi:10.1061/\(ASCE\)EM.1943-7889.0001163](https://doi.org/10.1061/(ASCE)EM.1943-7889.0001163).
- 515 [25] V. Šmilauer, et al., *Yade Documentation 2nd ed*, The Yade Project, 2015.
516 [doi:10.5281/zenodo.34073](https://doi.org/10.5281/zenodo.34073).
517 URL <http://yade-dem.org/doc/>
- 518 [26] L. Scholtès, P.-Y. Hicher, F. Nicot, B. Chareyre, F. Darve, On the capillary
519 stress tensor in wet granular materials, *International Journal for Numer-*
520 *ical and Analytical Methods in Geomechanics* 33 (10) (2009) 1289–1313.
521 [doi:10.1002/nag.767](https://doi.org/10.1002/nag.767).
- 522 [27] S. Herminghaus, Dynamics of wet granular matter, *Advances in Physics*
523 54 (3) (2005) 221–261. [doi:10.1080/00018730500167855](https://doi.org/10.1080/00018730500167855).
- 524 [28] J. Duriez, R. Wan, Subtleties in discrete-element modelling of wet granular
525 soils, *Géotechnique* 67 (4) (2017) 365–370. [doi:10.1680/jgeot.15.P.113](https://doi.org/10.1680/jgeot.15.P.113).
- 526 [29] I. F. Collins, The concept of stored plastic work or frozen elas-
527 tic energy in soil mechanics, *Géotechnique* 55 (5) (2005) 373–382.
528 [doi:10.1680/geot.2005.55.5.373](https://doi.org/10.1680/geot.2005.55.5.373).

- 529 [30] R. Puebla, A. Relaño, Irreversible processes without energy dissipation in
530 an isolated Lipkin-Meshkov-Glick model, *Phys. Rev. E* 92 (2015) 012101.
531 [doi:10.1103/PhysRevE.92.012101](https://doi.org/10.1103/PhysRevE.92.012101).
- 532 [31] M. Pouragha, R. Wan, Non-dissipative structural evolutions
533 in granular materials within the small strain range, *International Journal of Solids and Structures* 110111 (2017) 94 – 105.
534 [doi:10.1016/j.ijsolstr.2017.01.039](https://doi.org/10.1016/j.ijsolstr.2017.01.039).
- 536 [32] A. Madeo, F. dell’Isola, F. Darve, A continuum model for deformable,
537 second gradient porous media partially saturated with compressible fluids,
538 *Journal of the Mechanics and Physics of Solids* 61 (11) (2013) 2196 – 2211.
539 [doi:10.1016/j.jmps.2013.06.009](https://doi.org/10.1016/j.jmps.2013.06.009).
- 540 [33] E. Nikooee, G. Habibagahi, S. Hassanizadeh, A. Ghahramani, Effective
541 stress in unsaturated soils: A thermodynamic approach based on the in-
542 terfacial energy and hydromechanical coupling, *Transport in Porous Media*
543 96 (2) (2013) 369–396. [doi:10.1007/s11242-012-0093-y](https://doi.org/10.1007/s11242-012-0093-y).